Inventory of Supplemental Information

A TRPV Channel in *Drosophila* Motor Neurons Regulates Presynaptic Resting Ca^{2+} Levels, Synapse Growth, and Synaptic Transmission

Ching-On Wong, Kuchuan Chen, Yong Qi Lin, Yufang Chao, Lita Duraine, Zhongmin Lu, Wan Hee Yoon, Jeremy M. Sullivan, Geoffrey T. Broadhead, Charlotte J. Sumner, Thomas E. Lloyd, Gregory T. Macleod, Hugo J. Bellen, and Kartik Venkatachalam

Supplemental data

SUPPLEMENTAL EXPERIMENTAL PROCEDURES

Drosophila strains

The existing strains used in the study were *Canton-S*, w^{1118}, iav^{1} (Gong et al., 2004), iav^{3621} (Gong et al., 2004), iav^{1}; P[iav^{+}] (Gong et al., 2004), *Df(1)BSC276 /FM7h/Dp(2;Y)G*, *Y* (Df1) (Bloomington *Drosophila* Stock Center), *Df(1)ED6878 /FM7h* (Df2) (Bloomington *Drosophila* Stock Center), *Df(3L)Exel6120, P{XP-U}Exel6120/TM6B, Tb*^{1} (Df^{nan}) (Bloomington *Drosophila* Stock Center), *UAS-iav* (Kwon et al., 2010), *UAS-nan* (kind gift from Dr. Craig Montell, UCSB), *UAS-iav*$^{IR(JF01904)}$ (Bloomington *Drosophila* Stock Center), *ok371-GAL4* (Brand and Perrimon, 1993; Meyer and Aberle, 2006), *d42-GAL4* (Sweeney and Davis, 2002), *n-syb-GAL4* (Pauli et al., 2008), *mef2-GAL4* (Ranganayakulu et al., 1996), *ato-GAL4* (Hassan et al., 2000), *UAS-NaChBac* (Luan et al., 2006), *UAS-hTRPV1* (Marella et al., 2006), *UAS-lysozyme-KDEL::GFP* (Snapp et al., 2004), kum^{170} (Sanyal et al., 2005), *UAS-serca*$^{IR(JF01948)}$ (Bloomington *Drosophila* Stock Center), RyR^{16} (Sullivan et al., 2000), *UAS-itpr*$^{IR(JF01957)}$ (Bloomington *Drosophila* Stock Center), RyR^{24D03} (Gao et al., 2013), *canA1*$^{KO2-2}$ (*canA1*$^{-/-}$, (Nakai et al., 2011)), *UAS-canA1*$^{IR(JF01871)}$ (Bloomington *Drosophila* Stock Center), *UAS-canA1*^{FB5} (Dijkers and O'Farrell, 2007), *UAS-canA1*^{CA} (Dijkers and O'Farrell, 2007), *UAS-sgg*^{DN} (Bourouis, 2002), nan^{36a} (Kim et al., 2003), trp^{1} (Montell et al., 1985), $trp\gamma^{G4}$ (kind gift from Dr. Craig Montell, UCSB), $trpL^{302}$ (Niemeyer et al., 1996), *pain*^{GAL4} (Tracey et al., 2003), pyx^{3} (Lee et al., 2005), $trpA1^{1}$ (Kwon et al., 2008), $wtrw^{2}$ (Kwon et al., 2008), *futsch*^{N94} (Roos et al., 2000).

The iav^{1} allele was previously attributed to a premature STOP codon in the *iav* gene (C1363T leading to Q455X) (Gong et al., 2004). However, when we resequenced the

iav^{1} genomic DNA, we found that the actual mutation in the *iav* gene is C908T. We found that C1363 is not mutated in *iav*^{1}. Nevertheless, the lack of Iav protein in the *iav*^{1} chordotonal neurons (Figure S3A) indicates that this newly identified mutation also leads to the absence of Iav protein as described (Gong et al., 2004).

Fly husbandry and chemical feeding

All flies were reared at room temperature (~22°C). Except for the experiments with capsazepine feeding, all flies were raised in standard fly food (1 L of liquid fly food contained: 95 g agar, 275 g Brewer's yeast, 520 g of cornmeal, 110 g of sugar, 45 g of propionic acid, and 36 g of Tegosept was dissolved in 92 ml of 95% ethanol). For the drug feeding experiments, 2.5 g of instant fly food (formula 4-24 plain, Carolina Biological Supply Company) with an additional 0.5 g of inactive yeast was suspended in 6 mL water with capsazepine or the vehicle solvent (methanol (1% v/v)).

Image quantification

In some analyses, Z-series were exported as TIFF files into the Image-Pro Plus software (Media Cybernetics) for deconvolution and 3-dimensional reconstructions. Bouton volumes were determined after 3D reconstruction using available functions in Image-Pro Plus. For determining the area of the synaptic boutons, the total area stained by DLG was divided by the number of boutons at that NMJ. In the data shown in Figures 4G-4H, an "HRP-mask" was applied by isolating the signal of the relevant channel that overlapped with HRP using Image-Pro Plus.

NMJ Electrophysiology

NMJ electrophysiology was performed as described previously (Yao et al., 2009). Briefly, wandering third instar larvae were dissected in ice-cold, zero calcium HL-3 (70 mM NaCl, 5 mM KCl, 20 mM $MgCl_2$, 10 mM $NaHCO_3$, 115 mM sucrose, 5 mM trehalose, and 5 mM HEPES; pH 7.2.), and rinsed with HL-3 containing indicated Ca^{2+} concentration. The fillet was incubated in the latter solution for at least 3 minutes before recording. Recordings were made from body-wall muscles 6 (abdominal segment 3) with sharp electrodes filled with a 2:1 mixture of 2 M potassium acetate and 2 M potassium chloride. Data were collected only when resting membrane potential was below −60 mV. EJPs were evoked by directly stimulating the hemisegmental nerve through a glass capillary electrode (internal diameter, ~10 μm) at 0.2 Hz. Stimulus pulses were generated by pClamp 8 software (Axon Instruments Inc). The applied currents were 6 μA ± 3 with fixed stimulus duration at 0.3 ms. Twenty to thirty evoked EJPs were recorded for each muscle for analysis. Miniature EJP (mEJP) events were collected for 5 min. Both EJPs and mEJPs were amplified with an Axoclamp 2B amplifier (Axon Instruments, Foster City, CA) under bridge mode, filtered at 10 kHz and digitized at 10 kHz (for EJPs) and 40 kHz (mEJPs) respectively with pClamp 8.0. Experiments were performed at room temperature (20°C – 22°C).

EJPs and paired-pulse stimulation were analyzed with pClamp 8.0 software (Axon Instruments). The mEJPs were analyzed using the Mini Analysis Program (Synaptosoft Inc., Decatur, GA). The EJPs amplitudes were corrected by nonlinear summation (Feeney et al., 1998). The quantal content of evoked release was calculated from individual muscles by the ratio of the average EJP amplitude over the average mEJP

amplitude. The Ca^{2+} cooperativity of neurotransmission was calculated as described (Jan and Jan, 1976; Littleton et al., 1994).

Transmission electron microscopy

NMJ ultrastructural imaging was done as described previously (Yao et al., 2009). Briefly, wandering third instar larvae were filleted at room temperature in Ca^{2+} free HL-3 medium and subsequently fixed overnight in 2% paraformaldehyde/2.5% glutaraldehyde/0.1 M cacodylic acid (pH 7.2). The pre-fixed fillets were then processed inside a Ted Pella Bio Wave microwave with vacuum attachments. Samples were fixed again, followed by 3x water rinses, post-fixed with 2% aqueous osmium tetroxide, and 3 more rinses with Millipore water. A graded series of ethanol concentrations from 30-100% was incorporated as the initial dehydrant followed by propylene oxide as a final dehydrant. Samples were gradually infiltrated with 3 increasing propylene oxide and Embed 812 ratios up to full resin under vacuum. Samples were allowed to infiltrate in pure resin overnight on a rotator. The samples were embedded into flat silicone molds and cured in the oven at 62^{o}C for three days. The polymerized samples were sectioned and stained with 1% uranyl acetate for 10 minutes followed by lead citrate for 1 minute before TEM examination. TEM images were captured using a JEOL JEM 1010 transmission electron microscope with an AMT XR-16 mid-mount 16 mega-pixel digital camera.

Statistical analyses

Comparisons between pairs of datasets were made using Student's t-test. Multiple datasets were first compared using One-way ANOVA. Pairwise comparisons were made within the ANOVA test by applying the Bonferroni post-hoc correction.

STATISTICS (related to the data shown in all figures)

All values represent mean ±SEM

Figure 1G Bouton number: WT = 68.2±3, *iav*^{1} = 37.1±1.9; *iav*^{1}/Df1 = 37.6±2, and *iav*^{1}/Df2 = 37.7±3.3; *iav*^{3621} = 41±2.6; *iav*^{1}/*iav*^{3621} = 45.2±2.2; *iav*^{1}; P[*iav*$^{+}$] = 61±2.3 ; *UAS-iav*^{JR} = 58.3±3.9, *ok371-GAL4* = 69.5±4.7, *ok371>iav*^{JR} = 45.2±2.5

Figure 1H Bouton number: WT = 23.9±1.1, *iav*^{1} = 16.1±1, *iav*^{1};P[*iav*$^{+}$] = 21.1±1.1

Figure 1I Volume per bouton (μm^3): WT = 1±0.2, *iav*^{1} = 2.3±0.5, *iav*^{1}; P[*iav*$^{+}$] = 0.6±0.2

Figure 1J Bouton number: *iav*^{1}; *UAS-iav* = 39.5±3.0, *iav*^{1}; *ok371-GAL4* = 44.3±2.9, *iav*^{1}; *ok371>iav* = 58.1±2.5, *iav*^{1};;*d42-GAL4* = 40.8±3.3, *iav*^{1}; *d42>iav* = 64.9±4.1, *iav*^{1}; *ato-GAL4* = 37.8±3.4, *iav*^{1}; *ato>iav* = 42.5±3.2, *iav*^{1}, *mef2>iav* = 34.8±2.5

Figure 2J Bouton number: *iav*^{1}; *UAS-TRPV1* = 43.3±2.5, *iav*^{1}; *ok371>hTRPV1* = 67.7±3.2, *ok371>hTRPV1* = 67.2±6; *iav*^{1}; *ok371>hTRPV4* = 41.3±1.9; *iav*^{1}; *ok371>nan* = 40.9±2.8

Figure 2K Bouton number in *iav*^{1}*; ok371>hTRPV1*: 0 μM CPZ = 83.9±3.6, 100 μM CPZ = 74.4±2.2, 300 μM CPZ = 52.2±2.0

Figure 2L Bouton number in *iav*^{1};P[*iav*$^{+}$]: 0 μM CPZ = 64.3±3.2, 300 μM CPZ = 71.5±4.7

Figure 2M Bouton number: *UAS-NaChBac* = 65.9±4.2, iav^{1}; *UAS-NaChBac* = 40.9±3.7, *ok371>NaChBac* = 69.0±2.2, iav^{1}; *ok371>NaChBac* = 53.1±2.3

Figure 3E Number of Futsch loops per NMJ: iav^{1}; P[iav^{+}] = 5.9±0.4, iav^{1} = 2.9±0.5

Figure 4O Bouton numbers: *UAS-canA1*^{IR} = 72.6±5.1, *ok371>canA1*^{IR} = 47.7±2.2, iav^{1}*; ok371>canA1*^{IR} = 47.9±1.9

Figure 4P Bouton numbers: iav^{1}; *UAS-canA1*^{CA} = 42.9±1.6, iav^{1}; *ok371>canA1*^{CA} = 60.2±2.5, *UAS-canA1*^{CA} = 59.2±2.6, *ok371>canA1*^{CA} = 54.2±1.6

Figure 4Q Number of Futsch loops per NMJ: iav^{1}; *UAS-canA1*^{CA} = 3.6±0.4, iav^{1}; *ok371>canA1*^{CA} = 7.4±0.5, *UAS-canA1*^{CA} = 7.0±0.5, *ok371>canA1*^{CA} = 6.2±0.6

Figure 4R Bouton numbers: iav^{1}; *UAS-sgg*^{DN} = 42.1±1.9, iav^{1}*; ok371>sgg*^{DN} = 65.6±3.8, *UAS-sgg*^{DN} = 68.4±3.6, *ok371>sgg*^{DN} = 75.6±3.5

Figure 5J Bouton numbers: *UAS-serca*^{IR} = 66.1±1.9, *ok371>serca*^{IR} = 49.0±2.4, iav^{1}; *ok371>serca*^{IR} = 41.6±2.7, Kum^{170}/+ = 46.1±5.7; RyR^{16}/+ = 47.3±2.8, iav^{1}; RyR^{16}/+ = 41.4±1.9, *UAS-itpr*^{IR} = 66.8±2.7; *elav>itpr*^{IR} = 43.5±3.0, *ok371>itpr*^{IR} = 40.9±2.7, iav^{1}; *UAS-itpr*^{IR} = 41.6±2.9, iav^{1}; *ok371>itpr*^{IR} = 41.9±3.0

Figure 5K Relative bouton area, *UAS-serca*^{IR} = 1±0.06, *ok371>serca*^{IR} = 1.7±0.1, +/+ = 1±0.03, RyR^{16}/+ = 1.6±0.05

Figure 5L Bouton numbers: iav^{1} = 37.1±1.9, iav^{1}; RyR^{24D03}/+ = 52.1±1.8, RyR^{24D03}/+ = 46.5±2.1

Figure 5M Relative ER Ca^{2+} levels: Iav control = 0.97±0.06, Iav overexpressing = 0.49±0.04; TRPV1 control = 1±0.07, TRPV1 overexpressing = 0.46±0.05; TRPV4 control = 1±0.02, TRPV4 overexpressing = 0.88±0.06

Figure 7C Intensity Ratios (GCAMP5G;tdTomoato): At $[Ca^{2+}]_{ext}$ = 1.5 mM, WT = 0.102±0.014, *iav*^{1} = 0.112±0.026; $[Ca^{2+}]$ = 0.5 mM, WT = 0.112±0.012, *iav*^{1} = 0.070±0.015; $[Ca^{2+}]$ = 0 mM, WT = 0.101±0.013, *iav*^{1} = 0.059±0.009

Figure 7E EJP amplitudes: *iav*^{1}; [*iav*$^{+}$]= 25.8±2.7, *iav*^{1} = 12.4±1.1, *iav*^{1}/Df = 12.7±1.9, *iav*^{1}; *ok371>iav* = 25.5±2.5, *canA1*$^{-/+}$ = 24.1±4.6, *canA1*$^{-/Df\text{-}canA1}$ = 22.3±3.1

Figure 7F Quantal content: *iav*^{1}; P[*iav*$^{+}$] = 18.8±2.1, *iav*^{1} = 8.6±1.2, *iav*^{1}/Df1 = 8.8±1.1, *iav*^{1}; *ok371>iav* = 20.5±2.5

Figure 7G Relative quantal content: At $[Ca^{2+}]_{ext}$ = 0.25 mM, *iav*^{1}; P[*iav*$^{+}$] = 1±0.1, *iav*^{1} = 0.3±0.1; $[Ca^{2+}]$ = 0.4 mM, *iav*^{1}; P[*iav*$^{+}$] = 1±0.1, *iav*^{1} = 0.6±0.1; $[Ca^{2+}]$ = 0.75 mM, *iav*^{1}; P[*iav*$^{+}$] = 1±0.1, *iav*^{1} = 0.9±0.2

Figure 7I Paired-pulse ratio normalized to the genomic rescue mean (%): *iav*^{1}; P[*iav*$^{+}$] = 95.0±7.8, *iav*^{1} = 134.7±10.5, *iav*^{1}/Df1 = 142.9±12.5, *iav*^{1}; *ok371>iav* = 112.8±3.2

Figure 7J EJP amplitudes: *iav*^{1}; P[*iav*$^{+}$] = 25.8±2.7, *ok371>iav* = 40±3.6

Figure 7K Quantal content: *iav*^{1}; P[*iav*$^{+}$] = 18.8±1.9, *ok371>iav* = 30.9±2.0

Figure 7L Paired-pulse ratio normalized to the genomic rescue mean (%): *iav*^{1}; *ok371>iav* = 112.8±3.2, *ok371>iav* = 79.9±4.0

Figure S2G Bouton numbers: *canA1*$^{-/+}$ = 67.9±4.9, *canA1*$^{-/Df\text{-}canA1}$ = 45.2±3.4, *UAS-canA1*^{FB5} = 82.6±2.9, *ok371>UAS-canA1*^{FB5} = 53.3±2.7

Figure S2H Relative bouton areas: *UAS-canA1*^{IR} = 1±0.05, *ok371>canA1*^{IR} = 1.8±0.1, *canA1*$^{-/+}$ = 1±0.07, *canA1*$^{-/Df\text{-}canA1}$ = 2.0±0.3, *iav*^{1}*; ok371>canA1*^{CA} = 1±0.1, *iav*^{1}; *UAS-canA1*^{CA} = 1.5±0.1

Figure S2I Bouton numbers: WT = 68.2±3.0, *futsch*^{N94} = 49.4±1.8, *futsch*^{N94}; *UAS-canA1*^{CA} = 49.8±1.4; *futsch*^{N94}; *d42>canA1*^{CA} = 47.9±2.1

Figure S4A mEJP amplitudes: *iav*^{1}; P[*iav*$^{+}$] = 1.4±0.1, *iav*^{1} = 1.6±0.2, *iav*^{1}/Df1 = 1.4±0.1, *iav*^{1}; *ok371>iav* = 1.3±0.1, *ok371>iav* = 1.4±0.2, *canA1*$^{-/+}$ = 1.6±0.1, *canA1*$^{-/Df\text{-}canA1}$ = 1.55±0.05

Figure S4B mEJP frequencies: *iav*^{1}; P[*iav*$^{+}$] = 1.9±0.3, *iav*^{1} = 2.4±0.3, *iav*^{1}/Df1 = 2.2±0.3, *iav*^{1}; *ok371>iav* = 1.7±0.2, *ok371>iav* = 2.2±0.5

Figures S4C Quantal content: At $[Ca^{2+}]_{ext}$ = 0.25 mM, *iav*^{1}; P[*iav*$^{+}$] = 1.9±0. 2, *iav*^{1} = 0.6±0.1; $[Ca^{2+}]$ = 0.4 mM, *iav*^{1}; P[*iav*$^{+}$] = 10.6±0.7, *iav*^{1} = 5.9±0.5; $[Ca^{2+}]$ = 0.5 mM, *iav*^{1}; P[*iav*$^{+}$] = 18.8±1.9, *iav*^{1} = 8.6±1.1; $[Ca^{2+}]$ = 0.75 mM, *iav*^{1}; P[*iav*$^{+}$] = 26.9±2.5, *iav*^{1} = 24.3±3.8

Figure S5D SV number/bouton area: *iav*^{1}; P[*iav*$^{+}$] = 8.5±2.8, *iav*^{1} = 8.8±1.2

Figure S5E SV number/AZ length: *iav*^{1}; P[*iav*$^{+}$] = 9.3±1.1, *iav*^{1} = 9.5±1.9

Figure S5F SV diameter: *iav*^{1}; P[*iav*$^{+}$] = 38.9±0.7, *iav*^{1} = 38.9±0.9

Figure S5G Quantal content values from Figure S4C plotted in $\log_{10}$ scale.

Figure S5H Bouton numbers: *UAS-iav* = 67.3±3.8, *ok371>iav* = 44.8±2.0, *d42>iav* = 44.7±2.1

Figure S5I Number of Brp punctae per NMJ: *UAS-iav* = 474.4±21.9, *ok371>iav* = 513.6±33.0

SUPPLEMENTAL TABLE 1 (Related to Figure 1)

NMJ bouton counts in TRP mutants at larval A3 segment, muscles 6/7.

	Genotype	Bouton Count (mean ± S.E.M)
	WT (Canton-S)	68.2±3.0
TRPC	*trp*^{1}	68±3.2
	trpγ^{G4}	67.4±3.9
	trpL^{302}	71.4±4.8
TRPA	*pain*^{GAL4}	64.4±3.2
	pyx^{3}	71.8±5.0
	trpA1^{1}	68.4±4.5
	wtrw^{2}	63.9±4.5
TRPV	*nan*^{36a}/*Df*^{nan}	73.8±5.7
	iav^{1}	37.1±1.9

SUPPLEMENTAL REFERENCES

Bourouis, M. (2002). Targeted increase in shaggy activity levels blocks wingless signaling. Genesis *34*, 99-102.

Brand, A.H., and Perrimon, N. (1993). Targeted gene expression as a means of altering cell fates and generating dominant phenotypes. Development *118*, 401-415.

Dijkers, P.F., and O'Farrell, P.H. (2007). Drosophila calcineurin promotes induction of innate immune responses. Curr Biol *17*, 2087-2093.

Feeney, C.J., Karunanithi, S., Pearce, J., Govind, C.K., and Atwood, H.L. (1998). Motor nerve terminals on abdominal muscles in larval flesh flies, Sarcophaga bullata: comparisons with Drosophila. J Comp Neurol *402*, 197-209.

Gao, S., Sandstrom, D.J., Smith, H.E., High, B., Marsh, J.W., and Nash, H.A. (2013). Drosophila ryanodine receptors mediate general anesthesia by halothane. Anesthesiology *118*, 587-601.

Gong, Z., Son, W., Chung, Y.D., Kim, J., Shin, D.W., McClung, C.A., Lee, Y., Lee, H.W., Chang, D.J., Kaang, B.K.*, et al.* (2004). Two interdependent TRPV channel subunits, inactive and Nanchung, mediate hearing in *Drosophila*. J Neurosci *24*, 9059-9066.

Hassan, B.A., Bermingham, N.A., He, Y., Sun, Y., Jan, Y.N., Zoghbi, H.Y., and Bellen, H.J. (2000). atonal regulates neurite arborization but does not act as a proneural gene in the Drosophila brain. Neuron *25*, 549-561.

Jan, L.Y., and Jan, Y.N. (1976). Properties of the larval neuromuscular junction in Drosophila melanogaster. J Physiol *262*, 189-214.

Kim, J., Chung, Y.D., Park, D.Y., Choi, S., Shin, D.W., Soh, H., Lee, H.W., Son, W., Yim, J., Park, C.S., *et al.* (2003). A TRPV family ion channel required for hearing in *Drosophila*. Nature *424*, 81-84.

Kwon, Y., Shen, W.L., Shim, H.S., and Montell, C. (2010). Fine thermotactic discrimination between the optimal and slightly cooler temperatures via a TRPV channel in chordotonal neurons. J Neurosci *30*, 10465-10471.

Kwon, Y., Shim, H.S., Wang, X., and Montell, C. (2008). Control of thermotactic behavior via coupling of a TRP channel to a phospholipase C signaling cascade. Nat Neurosci *11*, 871-873.

Lee, Y., Lee, Y., Lee, J., Bang, S., Hyun, S., Kang, J., Hong, S.T., Bae, E., Kaang, B.K., and Kim, J. (2005). Pyrexia is a new thermal transient receptor potential channel endowing tolerance to high temperatures in Drosophila melanogaster. Nat Genet *37*, 305-310.

Littleton, J.T., Stern, M., Perin, M., and Bellen, H.J. (1994). Calcium dependence of neurotransmitter release and rate of spontaneous vesicle fusions are altered in Drosophila synaptotagmin mutants. Proc Natl Acad Sci U S A *91*, 10888-10892.

Luan, H., Lemon, W.C., Peabody, N.C., Pohl, J.B., Zelensky, P.K., Wang, D., Nitabach, M.N., Holmes, T.C., and White, B.H. (2006). Functional dissection of a neuronal network required for cuticle tanning and wing expansion in Drosophila. J Neurosci *26*, 573-584.

Marella, S., Fischler, W., Kong, P., Asgarian, S., Rueckert, E., and Scott, K. (2006). Imaging taste responses in the fly brain reveals a functional map of taste category and behavior. Neuron *49*, 285-295.

Meyer, F., and Aberle, H. (2006). At the next stop sign turn right: the metalloprotease Tolloid-related 1 controls defasciculation of motor axons in Drosophila. Development *133*, 4035-4044.

Montell, C., Jones, K., Hafen, E., and Rubin, G. (1985). Rescue of the Drosophila phototransduction mutation trp by germline transformation. Science *230*, 1040-1043.

Nakai, Y., Horiuchi, J., Tsuda, M., Takeo, S., Akahori, S., Matsuo, T., Kume, K., and Aigaki, T. (2011). Calcineurin and its regulator sra/DSCR1 are essential for sleep in Drosophila. J Neurosci *31*, 12759-12766.

Niemeyer, B.A., Suzuki, E., Scott, K., Jalink, K., and Zuker, C.S. (1996). The Drosophila light-activated conductance is composed of the two channels TRP and TRPL. Cell *85*, 651-659.

Pauli, A., Althoff, F., Oliveira, R.A., Heidmann, S., Schuldiner, O., Lehner, C.F., Dickson, B.J., and Nasmyth, K. (2008). Cell-type-specific TEV protease cleavage reveals cohesin functions in Drosophila neurons. Dev Cell *14*, 239-251.

Ranganayakulu, G., Schulz, R.A., and Olson, E.N. (1996). Wingless signaling induces nautilus expression in the ventral mesoderm of the Drosophila embryo. Dev Biol *176*, 143-148.

Roos, J., Hummel, T., Ng, N., Klambt, C., and Davis, G.W. (2000). Drosophila Futsch regulates synaptic microtubule organization and is necessary for synaptic growth. Neuron *26*, 371-382.

Sanyal, S., Consoulas, C., Kuromi, H., Basole, A., Mukai, L., Kidokoro, Y., Krishnan, K.S., and Ramaswami, M. (2005). Analysis of conditional paralytic mutants in

Drosophila sarco-endoplasmic reticulum calcium ATPase reveals novel mechanisms for regulating membrane excitability. Genetics *169*, 737-750.

Snapp, E.L., Iida, T., Frescas, D., Lippincott-Schwartz, J., and Lilly, M.A. (2004). The fusome mediates intercellular endoplasmic reticulum connectivity in Drosophila ovarian cysts. Mol Biol Cell *15*, 4512-4521.

Sullivan, K.M., Scott, K., Zuker, C.S., and Rubin, G.M. (2000). The ryanodine receptor is essential for larval development in Drosophila melanogaster. Proc Natl Acad Sci U S A *97*, 5942-5947.

Sweeney, S.T., and Davis, G.W. (2002). Unrestricted synaptic growth in *spinster*-a late endosomal protein implicated in TGF-β-mediated synaptic growth regulation. Neuron *36*, 403-416.

Tracey, W.D., Jr., Wilson, R.I., Laurent, G., and Benzer, S. (2003). painless, a Drosophila gene essential for nociception. Cell *113*, 261-273.

Yao, C.K., Lin, Y.Q., Ly, C.V., Ohyama, T., Haueter, C.M., Moiseenkova-Bell, V.Y., Wensel, T.G., and Bellen, H.J. (2009). A synaptic vesicle-associated Ca2+ channel promotes endocytosis and couples exocytosis to endocytosis. Cell *138*, 947-960.

Figure S1 (related to Figure 2)

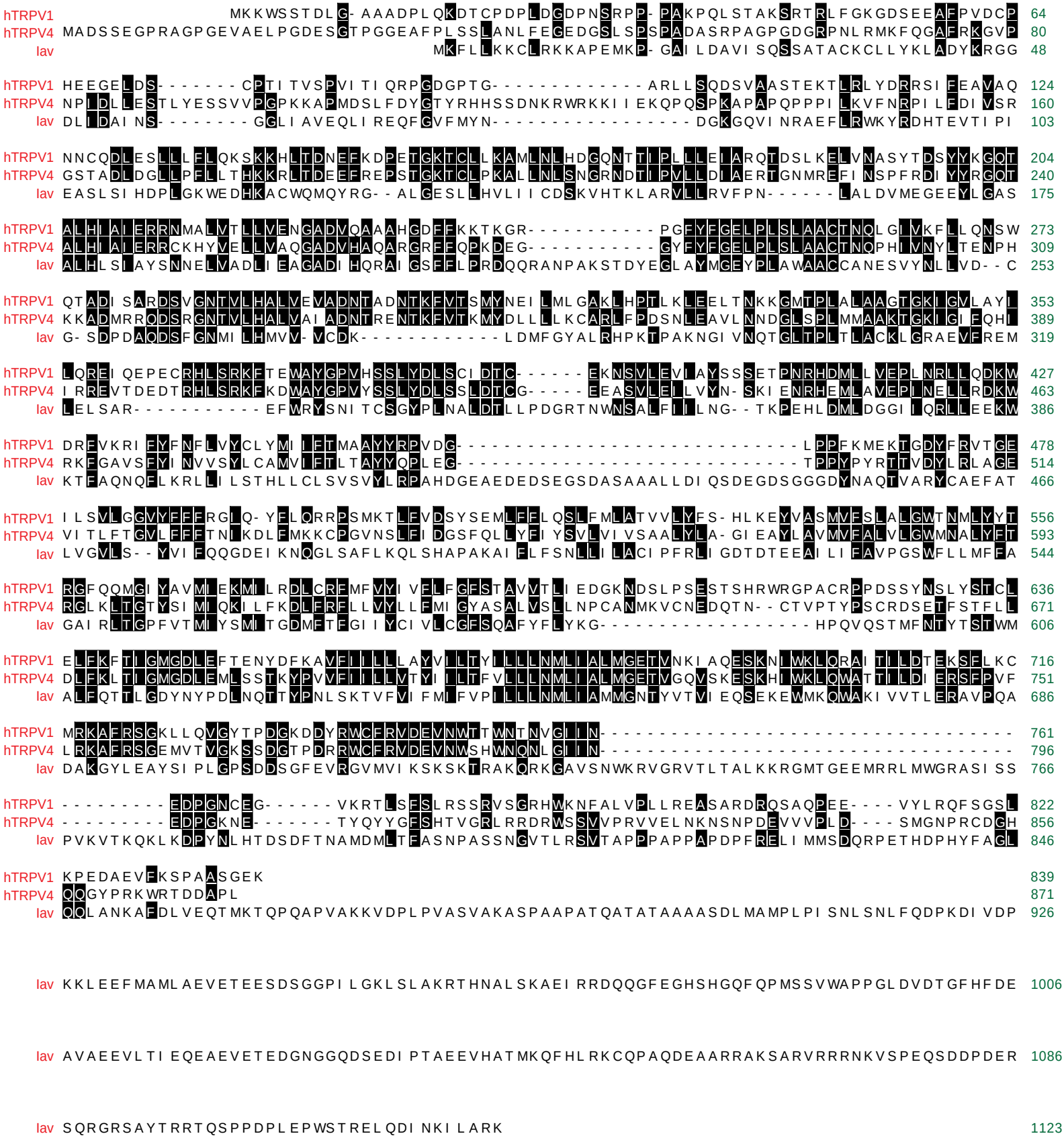

FIGURE S1. Alignment of the primary amino acid sequences of human TRPV1, human TRPV4, and *Drosophila* Iav. The numerical values on the right indicate the positions of the amino acids in the 3 proteins. Black shaded boxes indicate residues that are conserved in at least 2 of the 3 proteins being aligned.

Figure S2 (related to Figure 4)

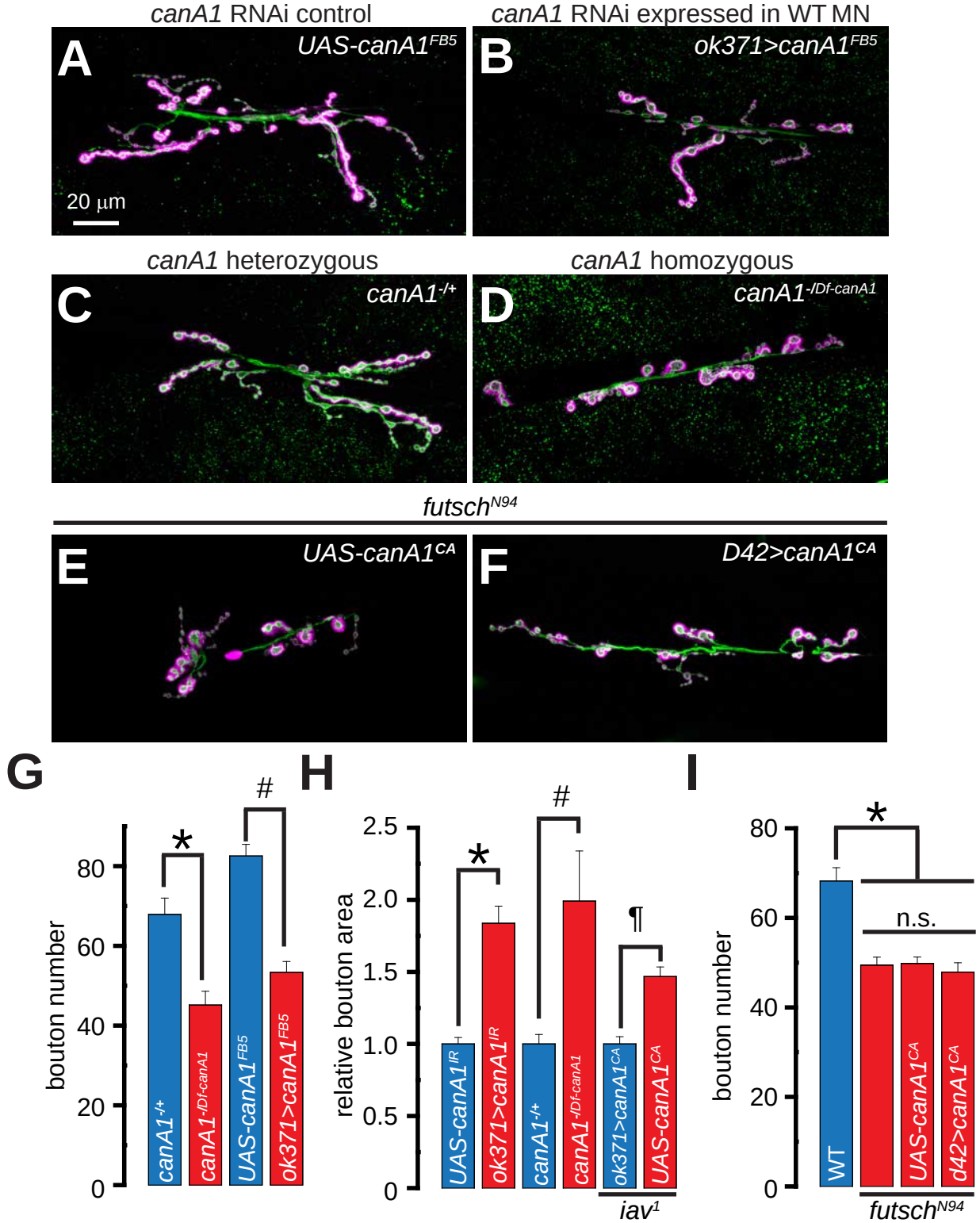

FIGURE S2. Calcineurin regulates NMJ bouton numbers and morphology via Futsch

(A-F) Representative confocal image of 3rd instar larval NMJs from larvae of the indicated genotypes stained with antibodies against the presynaptic marker, HRP (green) and the postsynaptic marker, DLG (magenta). Scale bar shown in (A) also applies to (B-F).

(G) Quantification of the NMJ bouton numbers in larvae of the indicated genotypes. *, $p = 5.4 \times 10^{-4}$, #, $p = 4.7 \times 10^{-6}$, unpaired Student's t-tests, n = 7-21 NMJs per genotype.

(H) Quantification of the relative bouton area in larvae of the indicated genotypes. *, $p = 1.7 \times 10^{-4}$; #, $p = 0.02$; ¶ = 3.4×10^{-5}; unpaired Student's t-tests, n =7-16 NMJs per genotype.

(I) Quantification of the NMJ bouton numbers in larvae of the indicated genotypes. *, $p = 9.3 \times 10^{-9}$, one-way ANOVA (comparing all the data sets), n = 16-30 NMJs per genotype.

All values represent mean ±SEM. Please consult the *Supplementary Files* for all values.

Abbreviations: WT, wild-type; MN, motor neuron.

Figure S3 (related to Figure 6)

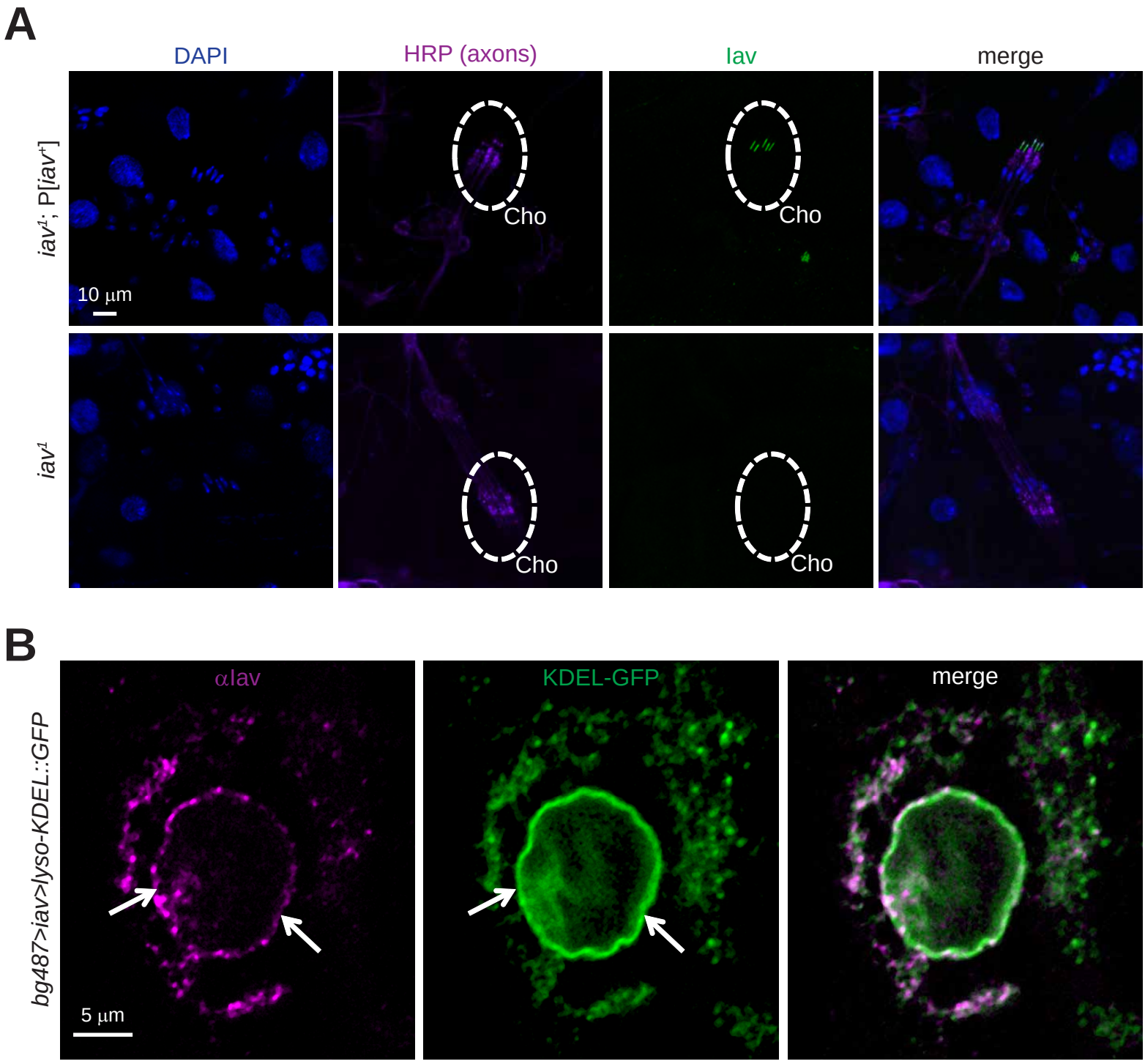

FIGURE S3. Iav expression in larval chordotonal neurons and muscle
(A) Representative confocal images of larval chordotonal neurons in larvae of the indicated genotypes stained with DAPI (blue), the neuronal marker, anti-HRP (purple), anti-Iav (green). *Dashed ovals* indicate chordotonal dendrites exhibiting Iav expression. Scale bar shown in the panel on the top-left applies to all panels.
(B) Representative confocal images of larval muscle of the indicated genotypes stained anti-Iav (magenta) and KDEL-GFP (green). *Arrows* indicate colocalization at the nuclear envelope. Scale bar shown in the panel on the left applies to all panels.

Figure S4 (related to Figure 7)

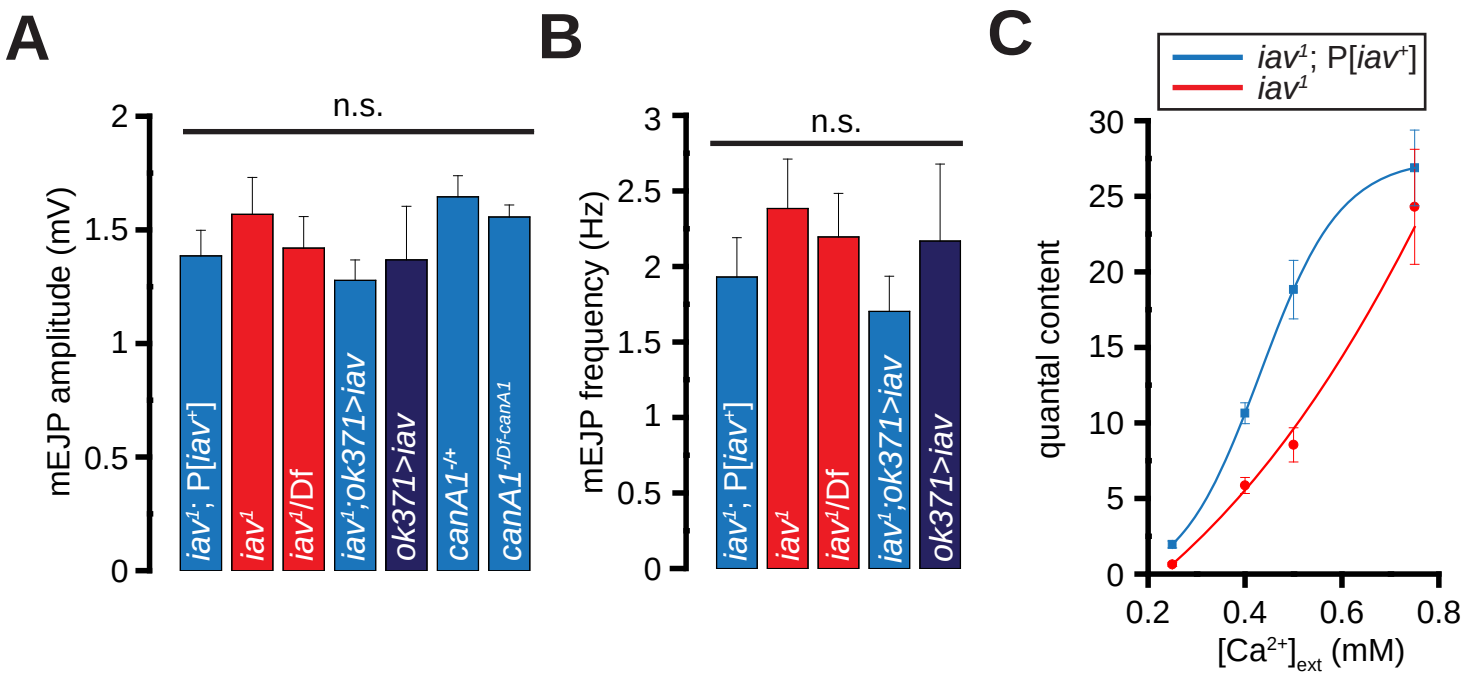

FIGURE S4. Alterations in evoked neurotransmission at the *iav*^{1} NMJs

(A) Quantification of the amplitude of the mEJPs obtained from recordings performed at 0.5 mM Ca^{2+} on larvae of the indicated genotypes.

(B) Quantification of the frequency of the mEJPs obtained from recordings performed at 0.5 mM Ca^{2+} on larvae of the indicated genotypes.

(C) Quantification of the quantal content obtained from recordings performed on larvae of the indicated genotypes at the indicated extracellular Ca^{2+} concentrations ($[Ca^{2+}]_{ext}$). The blue and red curves were obtained by fitting the respective mean values to sigmoidal functions using Origin6 (OriginLab corporation).

All values represent mean ±SEM. Please consult the *Supplementary Files* for all values and information on statistical tests employed. Abbreviations: n.s., not significant.

Figure S5 (related to Figure 7)

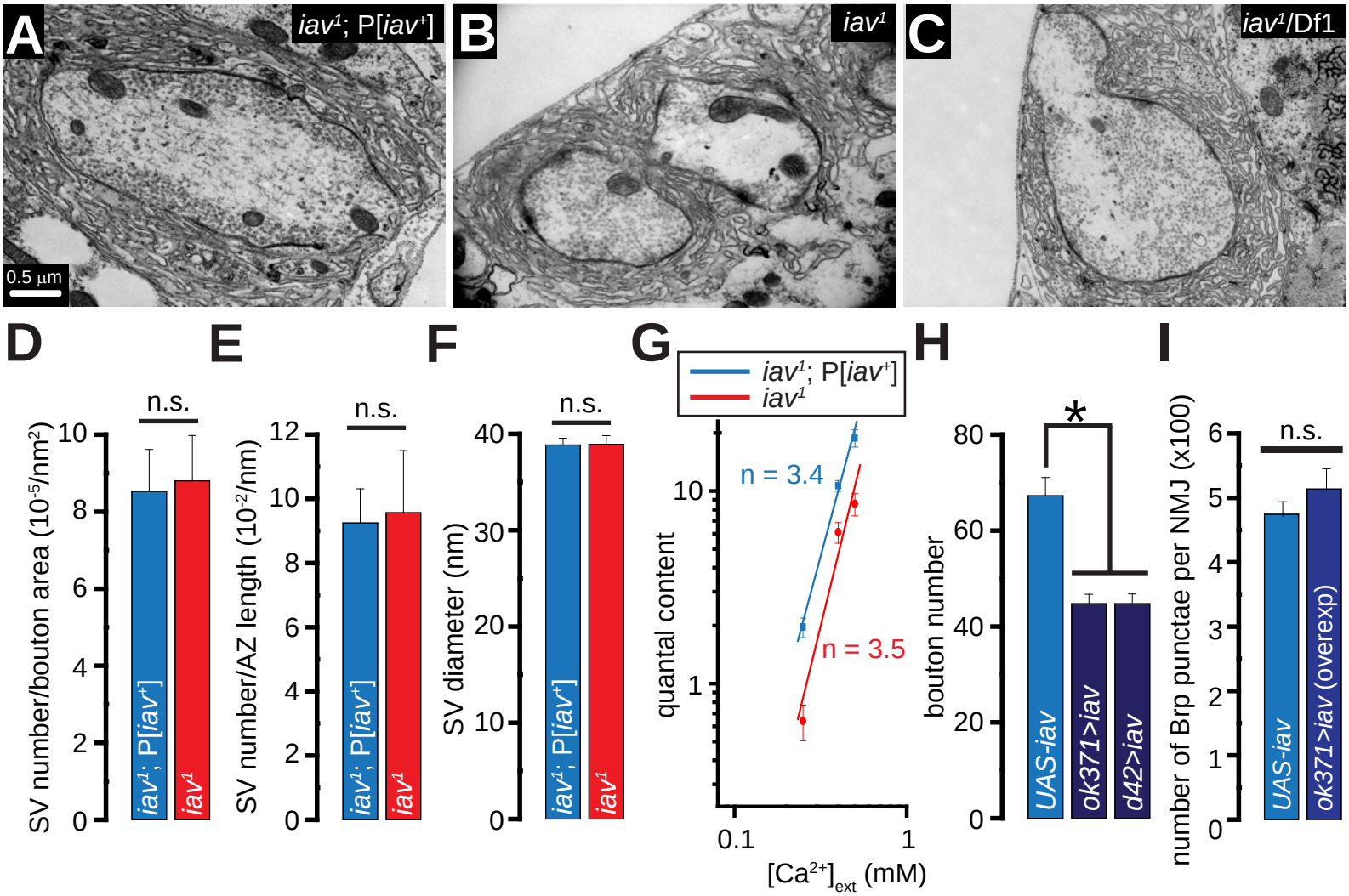

FIGURE S5. The *iav*^{1} synaptic boutons do not exhibit ultrastructural alterations in SV release machinery
(A-C) Transmission electron micrographs of boutons from muscle 6 of 3rd instar larvae of the indicated genotypes. Scale bar shown in (A) apply to (A-C).
(D-F) Quantification of then indicated parameters in the indicated genotypes.
(G) Quantification of the Ca^{2+} cooperativity of SV release in larvae of the indicated genotypes at the indicated extracellular Ca^{2+} concentrations ($[Ca^{2+}]_{ext}$). Both axes are in the $\log_{10}$ scale. The blue and red lines were obtained by linear fitting of the respective mean values using Origin6 (OriginLab corporation). “n” refers to the slope of the lines.
(H) Quantification of the bouton numbers in the indicated genotypes. *, $p = 1.01 \times 10^{-7}$, one-way ANOVA, n = 15-19 NMJs per genotype.
(I) Quantification of the number of Brp punctae per NMJ in larvae of the indicated genotypes.
All values represent mean ±SEM. Please consult the *Supplementary Files* for all values and information on statistical tests employed. Abbreviations: n.s., not significant.